NiCl2xBSc Manucsript 1

Title: Morphological and transcriptomic responses to acute nickel exposure in the colonial marine tunicate, *Botryllus schlosseri*.

Celeste Valdivia[1], Cindy Chou[2], Gina Jones[2], Dietmar Kültz[3], Baruch Rinkevich[4], Theo Bammler[5], James W. MacDonald[5], Alison M. Gardell[2,*]

[1]School of Aquatic and Fishery Sciences, University of Washington, Seattle, WA 98195, USA

[2]Department of Sciences and Mathematics, University of Washington Tacoma, Tacoma, WA 98402, USA

[3]Department of Animal Sciences & Genome Center, University of California Davis, Davis, California, USA

[4]Israel Oceanographic and Limnological Research, National Institute of Oceanography, Tel-Shikmona, Haifa 31080, Israel

[5]Genomics, Bioinformatics & Biostatistics, Microphysiological Systems Facility Core, University of Washington, Seattle, WA, USA

*Address correspondence to Alison Gardell (Email: agardell@uw.edu)

Acknowledgements: We thank Thanh Phuong Trinh for performing data collection for

Disclaimer: Funding provided through an NSF-BSF collaborative grant (BSF 2021650; NSF-MCB 2127516 and 2127517) awarded to B. Rinkevich, D. Kültz, and A. M. Gardell.

Data availability: Data and associated metadata are available upon request from the corresponding author (agardell@uw.edu).

Author Contributions statement: C. Valdivia and A. M. Gardell conceived and designed experiments. G. Jones conducted pilot studies. C. Valdivia performed laboratory experiments, performed statistical analyses, and wrote the manuscript. T. Bammler and J. W. MacDonald performed bioinformatics analyses. C. Chou assisted in the data analyses and collection. A. M. Gardell, B. Rinkevich, D. Kültz, T. Bammler, and J. W. MacDonald provided editorial assistance.

RUNNING HEAD: Nickel toxicity phenotypic and transcriptional responses in a colonial marine tunicate

TITLE: Morphological and transcriptomic responses to acute nickel exposure in the colonial marine tunicate, *Botryllus schlosseri*.

ABSTRACT:

Botryllus schlosseri is a globally distributed colonial marine tunicate and emerging model across developmental, immunological, and cellular studies; however, the species remains understudied within toxicological and stress physiological contexts. This study established the nickel tolerance of field-sourced *B. schlosseri* colonies and characterized morphological and transcriptomic responses following acute sublethal nickel (II) chloride exposure. Colonies exhibited a high tolerance to nickel with mortality only observed after 24-hours at the highest exposure concentration (1000 mg L^{-1} nominal $NiCl_2$). At 100 mg L^{1} nominal $NiCl_2$, colonies entered into blastogenic arrest after 24 hours which persisted for the entirety of the 96 hour exposure. Nickel exposure induced dose-dependent declines in health, with an increased frequency of phenotypic markers of stress in elevated concentrations of nickel exposure including: hyperpigmentation, reduced hemolymph flow, dilated extracorporeal vasculature, tunic degradation, and zooid cluster disruption. Differential gene expression analysis revealed a relatively constrained transcriptional response in late blastogenic stage (stage D) colonies exposed for 24-hours to $NiCl_2$ (nominal 100 mg L^{-1}) compared with unexposed stage D colonies, with only 54 genes differentially expressed across the two treatments. Genes involved in redox homeostasis, extracellular matrix (ECM) remodeling, vasculature dynamics, and modulation of cellular differentiation were upregulated in nickel exposed colonies. Notably, much of the transcriptomic signature of nickel exposed colonies closely corresponded to the

initiation of phenotypic changes in health such as reduced hemolymph movement, compromised tunic, and blastogenic arrest. Overall, these findings offer insights into the stress physiology of *B. schlosseri* through the identification of the nickel tolerance limits and associated underlying molecular stress-response mechanisms of this species.

KEYWORDS: nickel; transcriptomics; ECM; vasculature; blastogenesis; *Botryllus schlosseri*

1. INTRODUCTION

Marine invertebrates regularly face a broad suite of environmental stressors, owing to the dynamic nature of their environments. Among the key environmental factors contributing to stress in marine invertebrates are pollutants like trace metals, which have become ubiquitous in coastal habitats as a result of metal-based antifouling paints, mining operations, and industrial runoff (Hiscock, 2008; Kenworthy et al., 2018; Ya'la et al., 2025). Of these trace metal pollutants, nickel (Ni) is widely recognized for driving reactive oxygen species (ROS) accumulation and oxidative stress in marine invertebrates through dysregulation mitochondrial function alongside suppression of antioxidant systems (Blewett and Leonard, 2017; Brix et al., 2016; Stohs and Bagchi, 1994). Nickel is consistently present in global open-ocean surface waters at background concentrations of approximately 2-8 nM (0.1-0.5 μg L^{-1}) (John et al., 2022), and is projected to increase in coastal areas in proportion to continued anthropogenic inputs (Gauthier et al., 2021; Orihuela-García et al., 2023). As a result, nickel bioaccumulation and toxicity may become increasingly relevant for sessile marine invertebrates within polluted coastal habitats.

Nickel contamination can drive evolutionary adaptation and facilitate invasive species success by imposing significant physiological stress on native and colonizing species (Potet et al., 2018). In this context, the globally invasive marine tunicate *Botryllus schlosseri* is a

relevant system for exploring the physiological and molecular mechanisms underlying stress tolerance. While *B. schlosseri* is considered generally tolerant of environmental pollution (Gregorin et al., 2021; Naranjo et al., 1996), this species bioaccumulates trace metals at concentrations that are orders of magnitude higher than the surrounding seawater (Guillén Matus et al., 2024). Interestingly, nickel is among the least bioaccumulated trace metals in *B. schlosseri* despite its consistent presence in coastal seawater (Guillén Matus et al., 2024). Whether low nickel bioaccumulation in *B. schlosseri* is a result of active detoxification mechanisms or efficient excretion through ionoregulatory processes remains unresolved. Cadmium (Cd) and copper (Cu) exposure have been shown to induce transcriptional and enzymatic antioxidant responses in *B. schlosseri* (Franchi et al., 2017; Leprêtre and Kültz, 2025). Nickel elicits oxidative stress responses in other marine invertebrates (Blewett et al., 2016; Dallas et al., 2013; Wang and Wang, 2009), but it remains unclear how nickel may disrupt antioxidant defenses in *B. schlosseri*.

In addition to persisting amongst environmental stressors, *B. schlosseri* also tolerates recurrent endogenous oxidative stress as a result of its asexual reproductive cycle. As a colonial tunicate, *B. schlosseri*, forms colonies of genetically identical zooids through weekly and cyclical blastogenesis (Figure 1), a type of asexual budding that enables continuous regeneration and rapid colony expansion (Manni et al., 2019). Within the final blastogenic stage where buds takeover (TO) and assume the role of the next generation of zooids, senescent zooid apoptosis and degeneration drives intracellular accumulation of ROS (Cima et al., 2010; Franchi et al., 2017). While *B. schlosseri* tolerates and proliferates under recurrent oxidative stress during blastogenesis, it remains unknown how its redox physiology may respond to an acute and severe oxidative perturbation. Assessing responses of extreme nickel exposure

during late blastogenesis, when intrinsic oxidative burden is expected to be at its highest, offers an especially relevant context for examining antioxidant defenses in this species.

Our understanding of *B. schlosseri* stress responses at the molecular level remains limited, despite the extensive genomic and transcriptomic resources (Campagna et al., 2016; De Thier et al., 2024; Voskoboynik et al., 2013). Previous transcriptomic studies in *B. schlosseri* have largely focused on transcriptional profiling of immune and developmental related pathways in this species (Campagna et al., 2016; Oren et al., 2007; Ricci et al., 2016), leaving stress-responsive pathways understudied in comparison. Clarifying the transcriptional profile underlying stress responses in *B. schlosseri* colonies represents a critical step toward understanding how this species tolerates and adapts to environmental stress such as that associated with a high nickel exposure.

To address this, the present study combines molecular and organismal phenotyping to comprehensively assess nickel-induced stress responses in colonies of *B. schlosseri*. We initially characterized colony-level tolerance to increasing nickel concentrations and quantified changes in superoxide dismutase (SOD), a primary enzymatic antioxidant. We then examined transcriptomic responses following an acute nickel exposure during late blastogenesis. By joining morphological phenotypes, antioxidant activity, and global transcriptional responses, this study provides a multi-level framework that evaluates antioxidant function in a stress-tolerant marine invertebrate, advancing our broader mechanistic understanding of how marine organisms respond under increasing environmental stress.

2. MATERIALS AND METHODS

2.1 Animal Field Collection and Husbandry

Colonies of *Botryllus schlosseri*, consisting of at least 100 zooids, were collected from floating docks at the City of Des Moines Marina (47°23'51.18"N, 122°19'46.01"W), Des Moines, Washington, USA, where high abundance of colonies are observed year-round. Field collections were conducted between April and May 2024 for the range-finding experiment and between September and November 2024 for the RNA-seq experiment. *B. schlosseri* colonies growing on Pacific blue mussels (*Mytilus sp.*) were preferentially selected for collection, as mussels typically supported larger colonies and could be removed from the substrate without damaging the colony. Pacific blue mussels with adhered colonies were gently removed by hand from the sides of the floating docks up to 36 cm deep into the water column and transferred into 400 mL containers filled with marina seawater. Containers were placed in an empty cooler to reduce temperature fluctuations throughout the sampling period (~1-2-hours).

B. schlosseri were transported back to the University of Washington, Tacoma (30.7 km transportation distance) and immediately processed. Colonies were peeled from Pacific blue mussel shells using a clean stainless steel razor blade and transferred to a 15 cm glass petri dish filled with marina seawater for health evaluation under a stereomicroscope (Nikon, SMZ-745T). Only healthy colonies were kept for lab acclimation, which was visually determined using the following criteria: a flat and firm tunic, normal zooid star-system formations, and at least one area or point of ampullae extension. Colonies were then tied to 76.2 x 50.8 x 1.2 mm glass slides with a cotton thread. Tied colonies were drip acclimated for one hour to the artificial seawater (Red Sea Salt; Red Sea, USA) in the University of

Washington, Tacoma's recirculating artificial seawater system (RAS) (18 °C; pH 8.0; 30 ppt). Slides were then transferred into glass staining racks to maintain colonies vertically. Colonies were held at a stocking density of 12 genets per 5-liter plastic container in the RAS and fed every other day with a mixture of Liquid RotiRich (Florida Aqua Farms) and Reef Phytoplankton (Seachem). Colonies were cleaned with a soft brush to remove any food debris and algal growth surrounding the ampullae and surface of the tunic and re-tied to their glass slides as needed to encourage gliding and adherence to glass slides.

Colonies used in the range-finding study were acclimated to the RAS for 11 days prior to experimentation. At the 9-day acclimation mark, colonies with at least 2 star-systems adhered to the glass slide and in good observable health (flat, firm, and clear tunic; extended ampullae; normal pigmentation) were subdivided using a clean razor blade into single star-system colonial fragments (ramets). Ramets for all range-finding experiments had an average of 11 zooids (± 4).

Colonies used in the RNA-seq experiment were maintained in the RAS for 10 ± 3 days prior to exposure. During this period, blastogenic cycles were monitored to identify colonies entering stage B for ramet division. Colonies were starved at early stage C and exposures were initiated at late stage C to allow maturation toward stage D over the 24-hour exposure period.

2.2 Range-finding Exposure Study

To establish a sublethal dose for subsequent RNA-seq experiments, a range-finding exposure study was conducted. For all range-finding exposures, a stock solution of 1 g L^{-1} nickel (II) chloride anhydrous ($NiCl_2$; Sigma-Aldrich, Cat. No. 339350) was prepared in Milli-Q water (18.2 MΩ·cm resistivity). Experimental range-finding concentrations of nickel (II) chloride were selected on a logarithmic scale from 0.1 to 1000 mg L^{-1} as a result of relevant

literature (Trott et al., 1995), and previous pilot studies with *B. schlosseri* illustrating tolerance at lower concentrations (data not shown.) The stock solution was diluted to nominal nickel (II) chloride concentrations of 0.1, 1, 10, 100, and 1000 mg L^{-1} in freshly prepared, aerated artificial seawater (33 ppt, pH 8.2, 18 °C). After spiking with the appropriate volume of stock nickel (II) chloride, solutions were thoroughly mixed and left to equilibrate for 30 minutes. Aliquots of 250 mL were then distributed into exposure vessels (473 mL wide-mouth mason jars) and sampled for analytical chemistry and Ni concentration verification using inductively coupled plasma mass spectrometry (ICP-MS), using instrumentation available at the University of Washington, Tacoma.

B. schlosseri colonies adhered to glass slides, each containing two healthy ramets from the same genet, were transferred to exposure vessels and maintained in an environmental chamber (18 °C; 12:12 light:dark photoperiod). Colony health and survival were monitored over the 96-hour exposure period and were imaged under a stereomicroscope (Nikon, SMZ-745T) with a camera attachment (Excelis 4K Microscope Camera) at 24, 48, 72, and 96-hour timepoints. Mortality was defined by the absence of zooid body wall muscle responsiveness and cessation of hemolymph circulation. Ramets were removed at 24 and 96 hours using a sterile steel razor blade and snap-frozen for downstream analysis of superoxide dismutase (SOD) activity.

1.2.4 Superoxide Dismutase 1 Activity Assay

Superoxide dismutase 1 (SOD1) was isolated and quantified from cytosolic protein extracts using the colorimetric Invitrogen SOD Colorimetric Activity Kit (Cat. No. EIASODC), following the manufacturer's instructions. One unit (U) of SOD is defined as the amount of enzyme required to exhibit 50% dismutation of superoxide radicals under the assay

conditions. Absorbance was recorded at 450 nm using a microplate reader (SpectraMax iD3, Molecular Devices). SOD1 activity was measured in duplicate technical replicates per homogenate with absorbance recorded at 450 nm both prior to and following xanthine oxidase incubation using a microplate reader. For each well, the change in absorbance was calculated (ΔA450). Plate specific blank wells were included in each plate and mean blank ΔA450 values were calculated per plate and subtracted from all wells to generate blank-corrected absorbance values. A standard curve was generated for each plate using known SOD standards ranging from 0 to 2 U mL^{-1}. Because assay response is logarithmic, blank-corrected absorbance values were modeled as a function of the natural logarithm of known SOD activity. Plate-specific linear regressions were then used to calculate SOD activity (U mL^{-1}) for each unknown sample. Calculated SOD activity values were subsequently adjusted for dilution factor. Finally, SOD1 activity per mg of protein (U mg^{-1} protein) was calculated using the quantified values of protein concentration per homogenate from the BCA assay.

1.2.3 Total Protein Concentrations

Whole frozen *B. schlosseri* ramets were weighed out and then homogenized in liquid nitrogen using a pre-chilled, autoclaved pestle. The pulverized samples were then resuspended in cold 1X PBS (0.5 mL per 100 mg of tissue) and centrifuged at 1,500 × g for 10 min at 4 °C. The resulting supernatant was collected for cytosolic protein analysis.

Total cytosolic protein concentrations were quantified using the Pierce BCA Protein Assay Kit (Thermo Fisher Scientific; Cat. Nos. 23225, 23227) with bovine serum albumin standards (BSA), at 562 nm on a microplate reader. Standard curves were generated for each assay plate using BSA standards ranging from 0 to 2 mg L^{-1}. For each plate, the mean absorbance of blank wells was calculated and subtracted from all standards and samples prior

to model fitting. Plate-specific linear models were then fit to blank-corrected absorbance values as a function of known protein in mg L^{-1}. As mean blank subtraction normalized 0 mg L^{-1} standard technical replicates to ~0 absorbance, standard curves were fit through the origin (0,0) using a no-intercept linear model. This approach constrained the model to reflect expected relationship between protein concentration and absorbance after blank correction ($R^2 > 0.989$ per each plate). Protein concentrations of unknown samples were then calculated from the plate-specific slope and adjusted for dilution factor prior to downstream normalization of enzyme activity.

2.3 RNA-seq Experiment

Prior to the start of exposure, colonies of *B. schlosseri* were staged under a stereomicroscope and those with at least two ramets adhered to the glass slide, in stage C2, and in good health were selected to proceed in the study. Using a 1 g L^{-1} nickel (II) chloride stock solution, exposure vessels (473 mL wide-mouth mason jars) containing 250 mL of freshly prepared, aerated artificial seawater (33 ppt, pH 8.2) were spiked to a nominal concentration of 100 mg L^{-1} $NiCl_2$. Control artificial seawater (ASW, 33 ppt, pH 8.2) exposure vessels were prepared concurrently. The $NiCl_2$ solution was thoroughly mixed and allowed to equilibrate for 10 min, after which a 10-mL sample was collected from each vessel for quality assurance analyses. After exposure water preparation, colonies were transferred into exposure vessels containing either control ASW or $NiCl_2$-spiked ASW. Colonies were then placed in an environmental chamber (18 °C; 12:12 h light:dark photoperiod; 90% humidity) and left for 24-hours. At the end of the 24-h exposure period, colonies were removed from their exposure vessel and rinsed in triplicate with fresh artificial seawater to remove any remaining nickel. Colonies post-exposure were imaged using a stereomicroscope and camera attachment. Colony

ramets were preserved in RNAprotect Tissue Reagent (Qiagen; Cat. No. 76104) and stored at -80 °C until RNA extraction.

For RNA extraction, RNAprotect was removed from tubes before preserved ramets were pulverized in liquid nitrogen using a pre-chilled, autoclaved pestle. Total RNA was isolated with the RNeasy Mini Kit (Qiagen; Cat. No. 74104) following the manufacturer's protocol. RNA quality and integrity were assessed using an Agilent Bioanalyzer. From twelve biological replicates per treatment, the six samples per treatment with the most comparable RNA quality and yield were selected for sequencing.

2.4 RNA-seq Differential Gene Expression Analysis

Raw RNA-seq reads were processed using a standard transcriptomic workflow (Supplemental Figure 1). Briefly, reads were aligned to a *B. schlosseri* transcriptome (file in preparation for publication) using Salmon (Patro et al., 2017). Transcript counts were summarized to the gene level with the tximport package in Bioconductor (Soneson et al., 2015). Gene annotation was performed using eggNOG. Gene-level counts were filtered to remove lowly expressed genes and normalized for library size using the trimmed mean of M-values (TMM) method implemented in the edgeR package (Robinson and Oshlack, 2010). Normalized counts were then analyzed with the limma-voom pipeline (Law et al., 2014), which models the mean-variance relationship of log-transformed transcript counts and fits a weighted linear model to each gene. To account for within-group dissimilarity, sample-specific weights were estimated from regression residuals that measured how much each sample's expression deviated from its group mean across all genes; samples with larger deviations were down-weighted in the model. Differential expression between nickel-treated and control

colonies was tested using empirical Bayes-moderated *t*-statistics, with significance determined at a false discovery rate (FDR) < 0.1.

Unannotated DEGs were further processed using BLASTx against the UniProt Swiss-Prot database (release 2025_03). A custom BLAST database was constructed locally, and DEGs were queried with an E-value cutoff of $1E^{-20}$, retaining the top hit per sequence. BLAST output was parsed and merged with UniProt annotation tables to append gene symbols, protein descriptions, and organism information to previously unannotated sequences.

3. RESULTS

3.1 Chemical Analysis

Nickel concentrations in control and treatment artificial seawater samples were verified by ICP-MS following nitric acid digestion. Measured dissolved nickel concentrations increased proportionally with nominal nickel (II) chloride additions across all treatments (Supplemental Tables 1 and 2). ICP-MS analyses of field-sourced seawater collected in May 2025 from the City of Des Moines Marina (site of specimens collection) detected dissolved nickel at a mean concentration of 1.3 ± 1.9 µg L^{-1} (Ni-60, n = 6).

3.2 Phenotypic and Health Declines with Increasing Nickel

In nominal concentrations below 100 mg L^{-1}, changes in observable health markers were minimal (Figures 2 and 3B2-B5). Colonies in the 0.1 mg L^{-1} nominal $NiCl_2$ treatment maintained typical morphology including, active hemolymph circulation, normal clustering of zooid systems, flat and clear tunics, and zooid contractions to physical stimulation. The colonies in the 1 and 10 mg L^{-1} nominal $NiCl_2$ treatments exhibited similar, but moderate, declines in health over time, maintaining active hemolymph circulation and zooid response,

but, accumulating morphological indications of stress by 96 hpe, including hyperpigmentation, tunic puffing, and ampullar retraction, and ampullar dilation (Figure 3C2-B3).

All biological replicates in the 100 mg L^{-1} dose exhibited blastogenic arrest by 24 hpe, characterized by the halted development of primary buds, regardless of the blastogenic stage at which exposure began (Figure 3C2- C5). Colonies at this dose remained alive over the duration of the 96-hour exposure but displayed increasingly slowed hemolymph flow rate in the vasculature. Furthermore, in the 100 mg L^{-1} dose, colonies exhibited hyperpigmentation, puffed tunic, retraction and swelling of ampullae, and dissociation of typical star-system architecture. Mortality was observed only at the highest concentration tested (1000 mg L^{-1}) over the 96-hour exposure period. Exposure to 1000 mg $L^{-1}$of nominal nickel (II) chloride resulted in 100% mortality by 48 hpe (Figure 2).

3.3 Median Lethal Nickel Concentration Approximation

The median 24-hour lethal nickel concentration (LC_{50}) for *Botryllus schlosseri* was estimated from the nickel concentrations measured from stock solutions pre-exposure using ICP-MS and observed cumulative mortality after 24 and 96-hours of exposure. Because mortality was only observed at the highest concentration (ICP-MS measured mean 290 mg L^{-1}, SD = 30.1 mg L^{-1}), a full dose-response curve could not be modeled using traditional logistic or probit regression approaches. Instead, mortality proportions were plotted against the measured nickel concentrations, and an approximate LC_{50} value was interpolated graphically by connecting the observed data points with a linear trend line. This approach provides an estimated threshold concentration for acute lethality under the conditions tested and serves primarily to inform subsequent sublethal exposure assays rather than to define a statistically

modeled LC_{50} value. The 24-hour and 96-hour LC_{50} values were calculated to be 177 mg L^{-1} and 159 mg L^{-1} (about an 11% decrease) using a line of best fit (Supplemental Figure 2).

LC_{50} values for other marine invertebrates span similar concentrations (Supplemental Table 3). Most available nickel toxicity data for marine species is derived from mollusks, crustaceans, and echinoderms. Notably, nickel LC_{50} data for any tunicate species is absent from the literature.

3.4 Superoxide Dismutase 1 Activity

Superoxide dismutase 1 (SOD1) activity differed significantly among colonies exposed to different nickel concentrations (two-way ANOVA, $F = 3.47$, $p = 0.041$), with a moderate effect size (partial $\eta^2 = 0.14$) that indicates ~14% of the variance in SOD1 activity was attributable to nickel exposure (Figure 4). Neither exposure duration nor the interaction between time and concentration significantly influenced SOD1 activity ($p > 0.05$). Tukey-Kramer adjusted pairwise comparisons did not detect significant differences among concentrations ($p > 0.05$), although Fisher's LSD comparisons indicated higher mean SOD1 activity at 1 mg L^{-1} nominal $NiCl_2$ relative to both the control and 100 mg L^{-1} treatments ($p < 0.05$). Nickel exposure elicits a modest, non-monotonic SOD1 enzyme activity response in colonies of *B. schlosseri*, though variability among colonies limited the detection of pairwise differences following correction for multiple comparisons (Tukey-Kramer).

3.4 Sequencing and Quality Control

The samples were sequenced by NovoGene in paired-end mode (2 × 150 bp read length), yielding an average of 34.42 (± 6.25) million paired-end reads per sample. Quality control on the raw reads was performed using FastQC. Data quality was further ensured

through assessment using a multidimensional scaling (MDS) plot (Supplemental Figure 3). Nickel treated and control samples were somewhat separated along the first two dimensions of the MDS plot, although some overlap was observed with one nickel treated sample clustering near controls and vice versa (Supplemental Figure 3). Meta-data confirmed that the two outlier samples were not mislabeled or swapped. Influence of outlier samples on the differential expression analysis was mitigated by the weighted linear regression implemented through the limma-voom pipeline (Law et al., 2014), which down-weighted samples with greater within-group dissimilarity based on robust regression residuals.

Dimension 1 (dim1) captured 18% of the total explained variance, indicating a moderate but consistent transcriptional shift in response to nickel exposure. Control colonies were more widely distributed across dim1 suggesting greater within-group variability under baseline conditions. Dimension 2 (dim2), which explained 11% of the total variance, captures subtler but distinct expression dissimilarity between nickel-treated and control colonies.

3.5 Differential Gene Expression in Nickel Exposed Colonies

Prior to conducting differential gene expression analysis, genes with no or very low expression were filtered and removed from the data set, leaving 13,970 genes from a total of 16,959. Among the identified genes, only 15 were downregulated and 39 upregulated in nickel treated colonies relative to control (FDR < 0.1) (Figure 5). The heatmap analysis depicts distinct clustering of the nickel treated and non-treated samples. BlastX was performed against a non-restricted (nr) UniProt database to supplementally annotate gene terms (red text; Figure 5) outside of what was available through eggNOG. Of the limited DEG list, 69% were successfully annotated using the above-described procedure (37 of 54). The most significantly over- and under-expressed genes in the nickel-treated group were zinc metalloproteinase

NAS-13 (*nas13*) (logFC = 2.63; adjusted p-value < 0.05) and Collectin-11 (*colec11*) (logFC = -3.39; adjusted p-value < 0.05), respectively.

Extracellular matrix (ECM) organization emerged as the most prominent functional category comprising 30% of all the annotated DE genes (11 of 37, Figure 6). Nickel exposure increased the expression of several ECM components, including interstitial structural proteins such as collagen VI α3 (*col6a3*), SCO-spondin (*sspo*), fibrinogen C-domain–containing protein 1 (*fibcd1*), and LCE-family proteins. Nickel-exposed colonies upregulated FRAS1-related extracellular matrix protein 1 (*frem1*) and heparan sulfate proteoglycan 2 (*hspg2*) transcripts involved in basement membrane assembly and integrity. Several enzymes involved in extracellular matrix reassembly were differentially expressed. Chitinase 1 (*chit1*) was downregulated while matrix metalloproteinase-21 (*mmp21*) and *nas13* were upregulated.

Heme-binding protein 2 (*hebp2*), associated with oxygen transport and oxidative stress signaling, and cysteine dioxygenase type 1 (*cdo1*), a regulator of intracellular cystine, were strongly downregulated in nickel exposed colonies. In contrast, a transcript annotated for the vertebrate ATP binding cassette subfamily B member 11 (*abcb11*), was upregulated.

Nickel exposure induced significant differential expression of several genes associated with regenerative signaling in *B. schlosseri*. Transcripts within and associated with the transforming growth factor beta (TGF-β) pathway were notably upregulated including *tgf-β2*, a key cytokine regulating cellular differentiation and migration. Moreover, additional regulatory components of the TGF-β/BMP axis were also upregulated including a Kielin/Chordin-like protein (*kcp*) homolog and a *tle*/*gro* family corepressor homolog. Beyond TGF-β associated pathways, *jag1*, a ligand of the Notch signaling cascade, was similarly upregulated in nickel

exposed colonies. Collectively, these results represent an upregulation of multiple genes involved in developmental and differentiation signaling nickel exposure.

4. DISCUSSION

4.1 B. schlosseri is highly tolerant to nickel exposure

Experimental nickel exposure of field-sourced *B. schlosseri* revealed a pattern of high survivorship, despite an eventual onset of morphological malformations including disrupted colonial architecture, vascular dilation, increased pigmentation, and weakened tunic integrity (Figure 3). Crude-LC_{50} nickel estimates of 177 mg L^{-1} at 24 hpe and 159 mg L^{-1} at 96 hpe (Supplemental Figure 2), place *B. schlosseri* among the most nickel-tolerant marine invertebrates reported under full-strength artificial seawater conditions (Supplemental Table 3) (Bryant et al., 1985; Calabrese et al., 1973; Eisler and Hennekey, 1977; Florence et al., 1994; Hajimad and Vedamanikam, 2013). Although colonies survived under extremely high nickel concentrations, exposure to ≥100 mg L^{-1} nominal $NiCl_2$ induced distinct morphological changes beginning at 24-hpe including slowed hemolymph circulation, impeded primary bud development, failed zooid resorption, and overall blastogenic arrest (Figure 1.3A-3C). These phenotypes closely resemble those observed following exposure to other oxidative stressors in *B. schlosseri*. For example, treatment with butylated hydroxytoluene (BHT), UV-B irradiation, and ionizing radiation all result in vascular dilation, halted zooid resorption, and arrest of blastogenesis (Qarri et al., 2020; Rinkevich and Weissman, 1990; Voskoboynik et al., 2002; Voskoboynik et al., 2004).

Blastogenic progression in *B. schlosseri* is highly dependent on the coordinated apoptosis and phagocytic clearance of senescent zooids, which together enable the recycling of

remnant macromolecular and nutrient resources to developing stage D primary buds (Franchi et al., 2016; Voskoboynik et al., 2004). Within the context of nickel-induced blastogenic arrest, suspension of complete zooid resorption and further primary bud growth, may reduce the metabolic demand and thus ROS generation occurring with blastogenic development (Cima et al., 2010; Franchi et al., 2017). As such, nickel-induced blastogenic arrest may be a part of a broader colonial maintenance strategy that reduces oxidative burden, potentially safeguarding stem-cell niches from excessive oxidative damage to preserve future regenerative capacity (Qarri et al., 2020).

4.2 Modest non-monotonic response in SOD1 enzymatic activity with increasing nickel concentrations

Superoxide dismutase 1 (SOD1) is a primary cytosolic antioxidant enzyme that catalyzes the dismutation of superoxide radicals ($O_2^{\bullet -}$), a reactive oxygen species generated during normal cellular metabolism and elevated under oxidative stress (Sheng et al., 2014). Through conversion of superoxide into molecular oxygen (O_2) and hydrogen peroxide (H_2O_2), SOD1 functions as an upstream regulator of redox balance, with H_2O_2 subsequently detoxified by downstream antioxidant systems including catalase (CAT) and glutathione peroxidases (GPx) (Andrés et al., 2022). SOD1 enzymatic activity in *B. schlosseri* exhibited a non-monotonic pattern across increasing nickel treatments, with modest elevation at 1 mg L^{-1} nominal $NiCl_2$ (0.29 mg L^{-1} Ni-60) and relatively reduced activity at 100 mg L^{-1} (27.64 mg L^{-1} Ni-60) comparable to control colonies after 96 hours of exposure (Figure 4). Only one other study has quantified SOD activity in this species, in which colonies were transplanted across coastal sites within the Lagoon of Venice (Tasselli et al., 2017). After 22 days of transplantation, colonies displayed varying levels of antioxidant activity, with elevated SOD

activity for colonies transplanted to the more environmentally stressful location, characterized by higher temperature (17.7 °C), elevated pH (8.64), and a greater variety of competing benthic species (Tasselli et al., 2017). To our knowledge, this study represents the first direct quantification of SOD enzymatic activity in *B. schlosseri* colonies under controlled experimental chemical exposure. Together, these findings indicate that while SOD activity in *B. schlosseri* is responsive to environmental stress and moderate contaminant levels, activity is constrained with exposure to elevated nickel concentration.

Non-monotonic patterns of SOD activity across increasing nickel concentration after an extended exposure period have been observed in other marine invertebrates. In the copepod *Tigriopus japonicus*, SOD activity remained largely unchanged across nickel concentrations (0.125-3 mg L^{-1}) during the first four days of exposure (Wang and Wang, 2009). However, by day 12, SOD activity exhibited a non-monotonic pattern, with the highest activity observed at the intermediate nickel concentration (0.75 mg L^{-1}), while SOD activity at the highest concentration was comparable to that of lower-dose treatments (Wang and Wang, 2009). A similar trend was reported in Pacific abalone, where exposure to the highest tested concentration of $NiCl_2$ (nominal 0.4 mg L^{-1}) resulted in reduced SOD activity in hepatopancreas and gill tissues relative to lower concentrations (nominal 0.1 mg L^{-1}) after two weeks of exposure (Min et al., 2021). Although assessment of nickel-induced changes to SOD activity in the present study was limited to acute exposure (≤ 96-hours) rather than chronic, weeks-long treatments as in the studies above, the non-monotonic response observed here may represent a similar constraint in antioxidant functional capacity occurring over a shorter time frame at substantially higher nickel concentrations.

Notably, the absence of elevated SOD activity at the nominal 100 mg L^{-1} dose occurred concurrently with severe morphological disruption and health declines (Figure 2 and 3A-3C), illustrating that SOD antioxidant activity is not further increased with increased physiological severity. In contrast, the elevated SOD activity observed at the lower nickel concentration suggests that nickel exposure elicits at least moderate levels of oxidative stress in this species. Antioxidant response against nickel-driven oxidative stress at the evaluated elevated concentrations may rely on a shift away from active enzymatic defense towards broader physiological constraints that reduce overall metabolic demand and endogenous ROS production, such as that which occurs through blastogenic developmental arrest.

4.3 Transcriptional landscape of nickel-exposed colonies

In contrast to the pronounced phenotypic changes observed with high nickel-dose exposure (Figure 3A-3C), the transcriptional response under these conditions revealed a more subtle but coordinated modulation of transcriptional programs (Figures 5 and 6). Notably, some of the most striking features of the transcriptomic landscape were defined not by what differed, but by what remained unchanged between control and nickel-treated *B. schlosseri*. Although SOD enzymatic activity was elevated at the lower nickel concentration, indicating that nickel exposure can elicit oxidative stress in *B. schlosseri*, SOD activity in *B. schlosseri* colonies exposed to 100 mg L^{-1} was comparable to those in the control treatment. Consistent with this, differential gene expression analysis between control and 100 mg L^{-1} nominal $NiCl_2$-treated colonies revealed no increased transcription of primary antioxidants at this elevated dose. Comparisons of SOD enzymatic activity with *sod* transcription of *B. schlosseri* colonies transplanted across different sites in the Lagoon of Venice demonstrated a decoupling of transcriptional gene expression and enzymatic activity where increased *sod* transcription did

not occur at the most environmentally stressful site despite elevated SOD activity (Tasselli et al., 2017).

In the context of experimental nickel exposure in other marine invertebrates, nickel elicits upregulation of antioxidant defense associated transcripts (e.g. *sod*, glutathione-S-transferase [*gst*], catalase [*cat*], and several metallothiones [*mt*]) at lower environmentally relevant concentrations within the first 24-hours of exposure, with expression often declining over extended exposure durations (Banni et al., 2017; Dallas et al., 2013). Yet these canonical antioxidant pathways were not differentially expressed in our study. Instead, across both control and nickel-exposed colonies, antioxidant defense associated mechanisms were equally elevated, including transcripts encoding for *sod* and glutathione peroxidase (*gpx*), primary enzymatic antioxidants. Moreover, no differential expression of glutathione synthetase (*gss*) and glutamate-cysteine ligase modifier subunit (*gclm*) was observed in nickel-treated colonies, both of which are catalysts required for glutathione synthesis, the primary endogenous non-enzymatic antioxidant (Dickinson and Forman, 2002).

The lack of differential expression of antioxidant defenses in our data set could be a result of several competing, but non-mutually exclusive hypotheses. As both control and nickel-treated colonies were in late blastogenic stage D, a period of elevated oxidative stress, it may be that antioxidant networks operate at a constitutively elevated transcriptional baseline during late blastogenesis that are not further perturbed with exogenous oxidative challenge. Consistent with this hypothesis, *B. schlosseri* colonies have been found to exhibit molecular markers of persistent oxidative burden, with unusually high levels of 4-hydroxy-2-nonenal (HNE) adducted proteins across their proteomes (Kültz et al., 2025). HNE is a highly reactive electrophilic aldehyde generated through lipid peroxidation under oxidative stress that readily

forms covalent post-translational adducts with nucleophilic amino acid residues on proteins (Schneider et al., 2008). Alternatively, the evaluated nickel concentration (100 mg L^{-1}) may represent a sufficiently high exposure level to elicit a rapid but transient transcriptional induction of antioxidant defenses that had already been attenuated by the 24-hour sampling time point. This interpretation is consistent with transcriptional trends observed in other nickel-exposed marine invertebrates where antioxidant transcripts initially increase but decline with prolonged exposure to lower environmentally relevant nickel concentrations (Blewett and Wood, 2015).

Rather than broad differential expression of primary antioxidant enzymes or glutathione biosynthesis genes, nickel exposure resulted in selective modulation of redox-associated transcripts. Cysteine dioxygenase type 1 (*cdo1*) was significantly downregulated in nickel-exposed colonies. CDO1 catalyzes the oxidation of cysteine to cysteine sulfinic acid, the first step in taurine biosynthesis (Dominy et al., 2007). Taurine functions as an osmolyte, and in other marine invertebrates CDO1 is transcriptionally upregulated under both hypo- and hypertonic salinity stress (e.g., *Sinonovacula rivularis* and *Sinonovacula constricta*), reflecting CDO1's role in osmoregulation (Liang et al., 2025; Yihua et al., 2024). However, cysteine is one of the least abundant intracellular amino acids and is highly conserved within protein functional sites due to the unique nucleophilicity and metal-binding properties of its thiol group (-SH) (Poole, 2015). Given this constrained availability, downregulation of *cdo1* under nickel exposure may reflect a shift in cysteine allocation away from osmolyte synthesis and toward conservation for thiol-based redox buffering. This interpretation is consistent with mechanistic evidence from mammalian *in vitro* systems in which CDO overexpression in HepG2/C3A cells

reduced intracellular cysteine and glutathione pools, ultimately resulting in increased cadmium toxicity (Dominy et al., 2007).

The transcript annotated as ATP-binding cassette transporter subfamily B member 11 (*abcb11*) was significantly upregulated in nickel exposed colonies. While a vertebrate ABCB11 ortholog is absent in marine invertebrates (Luckenbach and Epel, 2008; Shipp and Hamdoun, 2012), the annotation likely represents an ABCB-like transporter, similar to those described in the sea urchin, *Strongylocentrotus purpuratus* (Shipp and Hamdoun, 2012). ABCB-family transporters in marine invertebrates broadly mediate efflux of metals, ions, and xenobiotics, with loss-of-function studies demonstrating that their disruption greatly impairs metal efflux capabilities (Della Torre et al., 2014; Vyas et al., 2022). In the context of nickel exposure in *B. schlosseri*, the lack of metallothionein transcriptional induction and upregulation of an ABCB-like transcript suggests that nickel handling and detoxification may rely more predominantly on transporter-mediated efflux than on thiol-based chelation. However, further functional studies are needed to confirm the centrality of efflux in this species' nickel detoxification response.

Nickel-exposed colonies showed upregulation of pathways associated with extracellular matrix (ECM) remodeling, basement membrane integrity, and vasculature dynamics. Differential expression of ECM- and adhesion-associated genes, including upregulation of matrix remodeling enzymes (e.g., *mmp21*, *nas13*), basement membrane components (e.g., *hspg2*, *frem1*), and vascular injury markers (*vwf*) (Oren et al., 2008), alongside downregulation of adhesion-associated transcripts (bves-like) (Brand, 2005; Osler et al., 2006), suggests compromised vascular and tunic barrier integrity coupled with compensatory structural reinforcement, which aligns with the observed ampullar dilation, slowed hemolymph

movement, and puffed tunic in exposed colonies. These findings indicate that nickel exposure elicits a coordinated ECM and epithelial remodeling response in *B. schlosseri*, affecting both interstitial matrix architecture and basement membrane domains. This aligns with previous work demonstrating the central role of ECM dynamics in maintaining tissue integrity, hemocyte migration, and blastogenic transitions during whole-body regeneration and metal-induced stress (Leprêtre and Kültz, 2025; Ricci et al., 2022).

Several genes associated with cell fate specification, developmental signaling, apoptosis regulation, and wound healing were significantly upregulated in nickel-exposed colonies, including components of the TGF-β superfamily and Notch signaling pathways. Within the TGF-β regulatory axis, transforming growth factor beta 2 (*tgf-β2*) and several modulators of TGF-β signaling were significantly upregulated in nickel-treated colonies, including syndecan binding protein (*sdcbp*), kielin/chordin-like protein (*kcp*), and transducin-like enhancer of split (*tle*). TGF-β2 is a cytokine involved in various processes of development and regeneration across vertebrates and invertebrates, regulating cellular differentiation, migration, and apoptosis (Lévesque et al., 2007; Wu and Hill, 2009). In the tunicate species *Botrylloides leachii* and *Ciona robusta*, upregulation of TGF-β and associated signaling enhancers play a critical role during initial wound healing and regeneration (Spina et al., 2017; Zondag et al., 2016). In *B. schlosseri*, inhibition of gene regulators in the TGF-β pathway results in colonial malformations including disrupted zooid architecture (Rosner et al., 2014), similar to the nickel-induced morphological disruptions observed in the present study. Together, this evidence indicates that the TGF-β axis is a conserved pathway across tunicates that is critical in regulating cellular differentiation, tissue growth, regeneration, and colonial structure.

While SDCBP is associated with TGF-β signal amplification (Zhang et al., 2025), KCP and TLE typically function as suppressors of TGF-β signaling and instead are enhancers of bone morphogenetic proteins (BMPs) (Lin et al., 2005; Zhang and Dressler, 2013; Zondag et al., 2016). In vertebrates, KCP is a secreted modulator of the TGF-β superfamily that antagonizes TGF-β signaling while enhancing BMP activity (Lin et al., 2005). TLE is also a well-recognized corepressor of TGF-β signaling in both mammalian systems (Zhang and Dressler, 2013), and invertebrate systems where TLE is homologous to groucho (GRO) (Zondag et al., 2016). Notably in the colonial tunicate *Botrylloides leachii*, *gro* downregulation (-3.1 fold) occurred concurrently with *tgfb2* upregulation (1.9 fold) during whole body regeneration (Zondag et al., 2016). This contrasting expression pattern between *B. leachii* undergoing active growth and *B. schlosseri* in a blastogenic arrested state suggests that transcriptional control of these cellular differentiation and tissue growth regulators can vary across developmental contexts but nevertheless converges on modulation of downstream developmental signaling pathways.

Modulation in cell fate signaling extended beyond the TGF-β pathway, where jagged1 *jag1*, a ligand in the Notch cascade (Grochowski et al., 2016), was significantly upregulated in nickel exposed colonies. Notch and TGF-β signaling are intimately connected but distinct pathways. In mammalian *in vitro* systems, TGF-β induces transcription of *jag1*, initiating downstream Notch signaling, which in turn confers a positive feedback loop by upregulating several TGF-β signaling components (Valdez et al., 2012; Zavadil and Cermak, 2004). The cross-talk between TGF-β and Notch signaling, has been proposed to be a key regulator of cellular quiescence (Niimi et al., 2007; Valdez et al., 2012), keeping cells from entering the cell cycle.

In addition to the transcriptional and phenotypic evidence of suspended cell growth for developing primary buds, *B. schlosseri* zooids also failed to be resorbed suggesting a disruption to the typical apoptotic and phagocytic clearance that occurs with blastogenesis. Consistent with this observation, programmed cell death 6 interacting protein (*pdcd6ip*) was upregulated in colonies exposed to nickel. PDCD6IP overexpression is involved in the activation of apoptosis pathways in mammalian systems (Strappazzon et al., 2010). Moreover, in stage D resorbing zooids of *B. schlosseri*, *pdcd6ip* is downregulated relative to active filter-feeding zooids, suggesting a potential association between PDCD6IP expression and the suppression of apoptosis during earlier blastogenic stages (Anselmi et al., 2023). Within this context, *pdcd6ip* upregulation in late blastogenic stage nickel-exposed colonies contrasts with the downregulation observed in stage D control colonies, suggesting a transcriptional shift consistent with the suspension of blastogenesis-associated apoptosis under exogenous oxidative stress.

Collectively, these transcriptional patterns suggest that nickel exposure perturbs highly conserved developmental signaling networks that coordinate the cellular differentiation, proliferation, and apoptosis underlying blastogenic takeover in this species. The simultaneous modulation of these pathways indicate that nickel stress may shift colonies toward a state of reduced cellular turnover, characterized by suspended apoptosis and halted developmental progression, consistent with the observed phenotypic changes observed during blastogenic arrest (Figure 2). These findings further support the proposed model in which *B. schlosseri* circumvents extensive antioxidant responses in favor of mitigating oxidative stress through modulation of colony-wide developmental programs that limit associated metabolic and oxidative activity. Within this framework, the coordinated modulation of transcriptional

cellular differentiation and apoptotic signaling may function to pause generational turnover, thereby reducing endogenous ROS generation and overall oxidative burden to preserve cellular integrity under elevated nickel exposure.

5. CONCLUSION

This study evaluated the heavy metal tolerance of *B. schlosseri* under acute nickel exposure. While colonies exhibited high survivorship even at elevated concentrations, this tolerance was accompanied by pronounced disruptions to physiological and developmental processes. Although colonies persisted in the second highest dose of nickel (II) chloride (100 mg L^{-1}), exposure resulted in halted primary bud growth progression, impaired hemolymph circulation, and failure of zooid resorption across all stages of the blastogenic cycle. Together, these phenotypic changes indicate that nickel exposure disrupts colony-level developmental processes associated with blastogenesis and generational turnover.

At the molecular scale, nickel elicited coordinated but limited transcriptional changes. Although antioxidant and genotoxic defenses associated with canonical metal response were not strongly induced by elevated nickel exposure, pathways associated with cysteine allocation and xenobiotic efflux were upregulated, signifying a limited detoxification response through metal sequestration. Instead, nickel exposure resulted in transcriptional changes to cellular differentiation and apoptotic signaling alongside restructuring of extracellular matrix and vasculature components. Collectively, these results suggest that colonies exposed to nickel during late blastogenesis rely less on transcriptional induction of classical antioxidant or DNA repair pathways and instead respond to nickel stress through modulation of developmental signaling and colony-wide remodeling. Such responses may stabilize cellular homeostasis under oxidative stress at the cost of colony structure and asexual reproduction. In *B. schlosseri*

this model has been proposed to specifically preserve long-term colonial viability and stem-cell lineages for similar-stress induced disruption to somatic tissues of the colony (Qarri et al., 2020; Svanfeldt et al., 2014).

REFERENCES

Andrés, C. M. C., Pérez De La Lastra, J. M., Juan, C. A., Plou, F. J. and Pérez-Lebeña, E. (2022). Chemistry of Hydrogen Peroxide Formation and Elimination in Mammalian Cells, and Its Role in Various Pathologies. *Stresses* 2, 256–274.

Anselmi, C., Caicci, F., Bocci, T., Guidetti, M., Priori, A., Giusti, V., Levy, T., Raveh, T., Voskoboynik, A., Weissman, I. L., et al. (2023). Multiple Forms of Neural Cell Death in the Cyclical Brain Degeneration of A Colonial Chordate. *Cells* 12, 1041.

Banni, M., Sforzini, S., Arlt, V. M., Barranger, A., Dallas, L. J., Oliveri, C., Aminot, Y., Pacchioni, B., Millino, C., Lanfranchi, G., et al. (2017). Assessing the impact of Benzo[a]pyrene on Marine Mussels: Application of a novel targeted low density microarray complementing classical biomarker responses. *PLOS ONE* 12, e0178460.

Blewett, T. A. and Leonard, E. M. (2017). Mechanisms of nickel toxicity to fish and invertebrates in marine and estuarine waters. *Environ. Pollut.* 223, 311–322.

Blewett, T. A. and Wood, C. M. (2015). Low salinity enhances NI-mediated oxidative stress and sub-lethal toxicity to the green shore crab (Carcinus maenas). *Ecotoxicol. Environ. Saf.* 122, 159–170.

Blewett, T. A., Smith, D. S., Wood, C. M. and Glover, C. N. (2016). Mechanisms of Nickel Toxicity in the Highly Sensitive Embryos of the Sea Urchin *Evechinus chloroticus* , and the Modifying Effects of Natural Organic Matter. *Environ. Sci. Technol.* 50, 1595–1603.

Brand, T. (2005). The Popeye Domain-Containing Gene Family. *Cell Biochem. Biophys.* 43, 095–104.

Brix, K. V., Schlekat, C. E. and Garman, E. R. (2016). The mechanisms of nickel toxicity in aquatic environments: An adverse outcome pathway analysis. *Environ. Toxicol. Chem.* 36, 1128–1137.

Bryant, V., Newbery, D. M., McLusky, D. S. and Campbell, R. (1985). (Corophiumv01Utator, Macoma balthica). *Mar Ecol Prog Ser*.

Calabrese, A., Collier, R. S., Nelson, D. A. and MacInnes, J. R. (1973). The toxicity of heavy metals to embryos of the American oyster Crassostrea virginica. *Mar. Biol.* 18, 162–166.

Campagna, D., Gasparini, F., Franchi, N., Vitulo, N., Ballin, F., Manni, L., Valle, G. and Ballarin, L. (2016). Transcriptome dynamics in the asexual cycle of the chordate Botryllus schlosseri. *BMC Genomics* 17, 275.

Cima, F., Manni, L., Basso, G., Fortunato, E., Accordi, B., Schiavon, F. and Ballarin, L. (2010). Hovering between death and life: Natural apoptosis and phagocytes in the blastogenetic cycle of the colonial ascidian Botryllus schlosseri. *Dev. Comp. Immunol.* 34, 272–285.

Dallas, L. J., Bean, T. P., Turner, A., Lyons, B. P. and Jha, A. N. (2013). Oxidative DNA damage may not mediate Ni-induced genotoxicity in marine mussels: Assessment of genotoxic

biomarkers and transcriptional responses of key stress genes. *Mutat. Res. Toxicol. Environ. Mutagen.* 754, 22–31.

De Thier, O., M.Tawfeeq, M., Faure, R., Lebel, M., Dru, P., Blanchoud, S., Alié, A., Brown, F. D., Flot, J.-F. and Tiozzo, S. (2024). First chromosome-level genome assembly of the colonial tunicate *Botryllus schlosseri*.

Della Torre, C., Bocci, E., Focardi, S. E. and Corsi, I. (2014). Differential ABCB and ABCC gene expression and efflux activities in gills and hemocytes of Mytilus galloprovincialis and their involvement in cadmium response. *Mar. Environ. Res.* 93, 56–63.

Dickinson, D. A. and Forman, H. J. (2002). Cellular glutathione and thiols metabolism. *Biochem. Pharmacol.* 64, 1019–1026.

Dominy, J. E., Hwang, J. and Stipanuk, M. H. (2007). Overexpression of cysteine dioxygenase reduces intracellular cysteine and glutathione pools in HepG2/C3A cells. *Am. J. Physiol.-Endocrinol. Metab.* 293, E62–E69.

Eisler, R. and Hennekey, R. J. (1977). Acute toxicities of Cd2+, Cr+6, Hg2+, Ni2+ and Zn2+ to estuarine macrofauna. *Arch. Environ. Contam. Toxicol.* 6, 315–323.

Florence, T. M., Stauber, J. L. and Ahsanullah, M. (1994). Toxicity of nickel ores to marine organisms. *Sci. Total Environ.* 148, 139–155.

Franchi, N., Ballin, F., Manni, L., Schiavon, F., Basso, G. and Ballarin, L. (2016). Recurrent phagocytosis-induced apoptosis in the cyclical generation change of the compound ascidian Botryllus schlosseri. *Dev. Comp. Immunol.* 62, 8–16.

Franchi, N., Ballin, F. and Ballarin, L. (2017). Protection from Oxidative Stress in Immunocytes of the Colonial Ascidian *Botryllus schlosseri* : Transcript Characterization and Expression Studies. *Biol. Bull.* 232, 45–57.

Gauthier, P. T., Blewett, T. A., Garman, E. R., Schlekat, C. E., Middleton, E. T., Suominen, E. and Crémazy, A. (2021). Environmental risk of nickel in aquatic Arctic ecosystems. *Sci. Total Environ.* 797, 148921.

Gregorin, C., Albarano, L., Somma, E., Costantini, M. and Zupo, V. (2021). Assessing the Ecotoxicity of Copper and Polycyclic Aromatic Hydrocarbons: Comparison of Effects on Paracentrotus lividus and Botryllus schlosseri, as Alternative Bioassay Methods. *Water* 13, 711.

Grochowski, C. M., Loomes, K. M. and Spinner, N. B. (2016). Jagged1 (JAG1): Structure, expression, and disease associations. *Gene* 576, 381–384.

Guillén Matus, D. G., Donaghy, C. M., Vijayan, N., Lane, Z. T., Howell, M., Glavin, G. G., Angeles-Boza, A. M., Nyholm, S. V. and Balunas, M. J. (2024). Multi-omics Analysis Reveals Important Role for Microbial-derived Metabolites from *Botryllus schlosseri* in Metal Interactions.

Hajimad, T. and Vedamanikam, J. (2013). Temperature effects on the toxicity of four trace metals to adult spotted Babylonia snails (*Babylonia areolata*). *Toxicol. Environ. Chem.* 95, 1380–1387.

Hiscock, K. (2008). *Star ascidian (Botryllus schlosseri): Marine Evidence–based Sensitivity Assessment (MarESA) Review*. Plymouth: Marine Biological Association of the United Kingdom.

John, S. G., Kelly, R. L., Bian, X., Fu, F., Smith, M. I., Lanning, N. T., Liang, H., Pasquier, B., Seelen, E. A., Holzer, M., et al. (2022). The biogeochemical balance of oceanic nickel cycling. *Nat. Geosci.* 15, 906–912.

Kenworthy, J. M., Rolland, G., Samadi, S. and Lejeusne, C. (2018). Local variation within marinas: Effects of pollutants and implications for invasive species. *Mar. Pollut. Bull.* 133, 96–106.

Kültz, D., Gardell, A. M., DeTomaso, A., Stoney, G., Rinkevich, B., Qarri, A. and Hamar, J. (2025). Proteome‐Wide 4‐Hydroxy‐2‐Nonenal Signature of Oxidative Stress in the Marine Invasive Tunicate *Botryllus schlosseri*. *PROTEOMICS* 25, 12–25.

Law, C. W., Chen, Y., Shi, W. and Smyth, G. K. (2014). voom: precision weights unlock linear model analysis tools for RNA-seq read counts. *Genome Biol.* 15, R29.

Leprêtre, M. and Kültz, D. (2025). Copper-induced stress and recovery impacts on organismal phenotypes and the underlying proteomic signatures in Botryllus schlosseri. *Sci. Total Environ.* 1004, 180803.

Lévesque, M., Gatien, S., Finnson, K., Desmeules, S., Villiard, É., Pilote, M., Philip, A. and Roy, S. (2007). Transforming Growth Factor: β Signaling Is Essential for Limb Regeneration in Axolotls. *PLoS ONE* 2, e1227.

Liang, J., Wei, Y., Liu, H., Liang, S., Li, Y., Zhou, Z. and Guo, Y. (2025). Study on the physiological and molecular regulatory mechanisms of Sinonovacula rivularis in response to low-salinity stress. *Aquac. Rep.* 45, 103174.

Lin, J., Patel, S. R., Cheng, X., Cho, E. A., Levitan, I., Ullenbruch, M., Phan, S. H., Park, J. M. and Dressler, G. R. (2005). Kielin/chordin-like protein, a novel enhancer of BMP signaling, attenuates renal fibrotic disease. *Nat. Med.* 11, 387–393.

Luckenbach, T. and Epel, D. (2008). ABCB- and ABCC-type transporters confer multixenobiotic resistance and form an environment-tissue barrier in bivalve gills. *Am. J. Physiol.-Regul. Integr. Comp. Physiol.* 294, R1919–R1929.

Manni, L., Anselmi, C., Cima, F., Gasparini, F., Voskoboynik, A., Martini, M., Peronato, A., Burighel, P., Zaniolo, G. and Ballarin, L. (2019). Sixty years of experimental studies on the blastogenesis of the colonial tunicate Botryllus schlosseri. *Dev. Biol.* 448, 293–308.

Min, E. Y., Kim, J.-H., Lee, J. S. and Kang, J.-C. (2021). Nickel bioaccumulation and the antioxidant response in Pacific abalone Haliotis discus hannai, Ino 1953 exposed to waterborne nickel during thermal stress. *Aquac. Rep.* 20, 100726.

Naranjo, S. A., Carballo, J. L. and Garcia-Gomez, J. C. (1996). Effects of environmental stress on ascidian populations in Algeciras Bay (southern Spain). Possible marine bioindicators? *Mar. Ecol. Prog. Ser.* 144: 119–131, 1996,.

Niimi, H., Pardali, K., Vanlandewijck, M., Heldin, C.-H. and Moustakas, A. (2007). Notch signaling is necessary for epithelial growth arrest by TGF-β. *J. Cell Biol.* 176, 695–707.

Oren, M., Douek, J., Fishelson, Z. and Rinkevich, B. (2007). Identification of immune-relevant genes in histoincompatible rejecting colonies of the tunicate Botryllus schlosseri. *Dev. Comp. Immunol.* 31, 889–902.

Oren, M., Escande, M., Paz, G., Fishelson, Z. and Rinkevich, B. (2008). Urochordate Histoincompatible Interactions Activate Vertebrate-Like Coagulation System Components. *PLoS ONE* 3, e3123.

Orihuela-García, M. A., Bolado-Penagos, M., Sala, I., Tovar-Sánchez, A., García, C. M., Bruno, M., Echevarría, F. and Laiz, I. (2023). Trace metals distribution between the surface waters of the Gulf of Cadiz and the Alboran Sea. *Sci. Total Environ.* 858, 159662.

Osler, M. E., Smith, T. K. and Bader, D. M. (2006). *Bves* , a member of the *Popeye* domain‐containing gene family. *Dev. Dyn.* 235, 586–593.

Patro, R., Duggal, G., Love, M. I., Irizarry, R. A. and Kingsford, C. (2017). Salmon provides fast and bias-aware quantification of transcript expression. *Nat. Methods* 14, 417–419.

Poole, L. B. (2015). The basics of thiols and cysteines in redox biology and chemistry. *Free Radic. Biol. Med.* 80, 148–157.

Potet, M., Giambérini, L., Pain-Devin, S., Louis, F., Bertrand, C. and Devin, S. (2018). Differential tolerance to nickel between Dreissena polymorpha and Dreissena rostriformis bugensis populations. *Sci. Rep.* 8, 700.

Qarri, A., Rosner, A., Rabinowitz, C. and Rinkevich, B. (2020). UV-B radiation bearings on ephemeral soma in the shallow water tunicate Botryllus schlosseri. *Ecotoxicol. Environ. Saf.* 196, 110489.

Ricci, L., Chaurasia, A., Lapébie, P., Dru, P., Helm, R. R., Copley, R. R. and Tiozzo, S. (2016). Identification of differentially expressed genes from multipotent epithelia at the onset of an asexual development. *Sci. Rep.* 6, 27357.

Ricci, L., Salmon, B., Olivier, C., Andreoni-Pham, R., Chaurasia, A., Alié, A. and Tiozzo, S. (2022). The Onset of Whole-Body Regeneration in Botryllus schlosseri: Morphological and Molecular Characterization. *Front. Cell Dev. Biol.* 10, 843775.

Rinkevich, B. and Weissman, I. L. (1990). *Botryllus schlosseri* (tunicata) whole colony irradiation: Do senescent zooid resorption and immunological resorption involve similar recognition events? *J. Exp. Zool.* 253, 189–201.

Robinson, M. D. and Oshlack, A. (2010). A scaling normalization method for differential expression analysis of RNA-seq data. *Genome Biol.* 11, R25.

Rosner, A., Alfassi, G., Moiseeva, E., Paz, G., Rabinowitz, C., Lapidot, Z., Douek, J., Haim, A. and Rinkevich, B. (2014). The involvement of three signal transduction pathways in botryllid ascidian astogeny, as revealed by expression patterns of representative genes. *Int. J. Dev. Biol.* 58, 677–692.

Schneider, C., Porter, N. A. and Brash, A. R. (2008). Routes to 4-Hydroxynonenal: Fundamental Issues in the Mechanisms of Lipid Peroxidation. *J. Biol. Chem.* 283, 15539–15543.

Sheng, Y., Abreu, I. A., Cabelli, D. E., Maroney, M. J., Miller, A.-F., Teixeira, M. and Valentine, J. S. (2014). Superoxide Dismutases and Superoxide Reductases. *Chem. Rev.* 114, 3854–3918.

Shipp, L. E. and Hamdoun, A. (2012). ATP‐binding cassette (ABC) transporter expression and localization in sea urchin development. *Dev. Dyn.* 241, 1111–1124.

Soneson, C., Love, M. I. and Robinson, M. D. (2015). Differential analyses for RNA-seq: transcript-level estimates improve gene-level inferences. *F1000Research* 4, 1521.

Spina, E. J., Guzman, E., Zhou, H., Kosik, K. S. and Smith, W. C. (2017). A microRNA-mRNA expression network during oral siphon regeneration in *Ciona*. *Development* 144, 1787–1797.

Stohs, S. J. and Bagchi, D. (1994). Oxidative Mechanisms in the Toxicity of Metal Ions. *Free Radic. Biol. Med.* 19, 321–336.

Strappazzon, F., Torch, S., Chatellard-Causse, C., Petiot, A., Thibert, C., Blot, B., Verna, J.-M. and Sadoul, R. (2010). Alix is involved in caspase 9 activation during calcium-induced apoptosis. *Biochem. Biophys. Res. Commun.* 397, 64–69.

Svanfeldt, K., Lundqvist, L., Rabinowitz, C., Sköld, H. N. and Rinkevich, B. (2014). Repair of UV-induced DNA damage in shallow water colonial marine species. *J. Exp. Mar. Biol. Ecol.* 452, 40–46.

Tasselli, S., Ballin, F., Franchi, N., Fabbri, E. and Ballarin, L. (2017). Expression of genes involved in oxidative stress response in colonies of the ascidian Botryllus schlosseri exposed to various environmental conditions. *Estuar. Coast. Shelf Sci.* 187, 22–27.

Trott, D. A., Cuthbert, A. P., Overell, R. W., Russo, I. and Newbold, R. F. (1995). Mechanisms involved in the immortalization of mammalian cells by ionizing radiation and chemical carcinogens. *Carcinogenesis* 16, 193–204.

Valdez, J. M., Zhang, L., Su, Q., Dakhova, O., Zhang, Y., Shahi, P., Spencer, D. M., Creighton, C. J., Ittmann, M. M. and Xin, L. (2012). Notch and TGFβ Form a Reciprocal Positive Regulatory Loop that Suppresses Murine Prostate Basal Stem/Progenitor Cell Activity. *Cell Stem Cell* 11, 676–688.

Voskoboynik, A., Reznick, A. Z. and Rinkevich, B. (2002). Rejuvenescence and extension of an urochordate life span following a single, acute administration of an anti-oxidant, butylated hydroxytoluene. *Mech. Ageing Dev.* 123, 1203–1210.

Voskoboynik, A., Rinkevich, B., Weiss, A., Moiseeva, E. and Reznick, A. Z. (2004). Macrophage involvement for successful degeneration of apoptotic organs in the colonial urochordate *Botryllus schlosseri*. *J. Exp. Biol.* 207, 2409–2416.

Voskoboynik, A., Neff, N. F., Sahoo, D., Newman, A. M., Pushkarev, D., Koh, W., Passarelli, B., Fan, H. C., Mantalas, G. L., Palmeri, K. J., et al. (2013). The genome sequence of the colonial chordate, Botryllus schlosseri. *eLife* 2, e00569.

Vyas, H., Schrankel, C. S., Espinoza, J. A., Mitchell, K. L., Nesbit, K. T., Jackson, E., Chang, N., Lee, Y., Warner, J., Reitzel, A., et al. (2022). Generation of a homozygous mutant drug transporter (ABCB1) knockout line in the sea urchin *Lytechinus pictus*. *Development* 149, dev200644.

Wang, M. and Wang, G. (2009). Oxidative damage effects in the copepod Tigriopus japonicus Mori experimentally exposed to nickel. *Ecotoxicology* 19, 273–284.

Wu, M. Y. and Hill, C. S. (2009). TGF-β Superfamily Signaling in Embryonic Development and Homeostasis. *Dev. Cell* 16, 329–343.

Ya'la, Z., Dewi, T., Husni, A., Santoso, T., Ndobe, S., Rosyida, E., Maemunah, M., Mappatoba, M. and Nurdin, M. (2025). Assessment of Heavy Metal Contaminations in Coastal Sediments due to Nickel Mining Activities in Morowali Regency Central Sulawesi Indonesia. *J. Min. Environ.* 16,.

Yihua, C., Min, D., Zhiguo, D., Yifeng, L. and Donghong, N. (2024). Function of taurine and its synthesis-related genes in hypertonic regulation of Sinonovacula constricta. *Comp. Biochem. Physiol. A. Mol. Integr. Physiol.* 287, 111536.

Zavadil, J. and Cermak, L. (2004). Integration of TGF-b/Smad and Jagged1/Notch signalling in epithelial-to-mesenchymal transition.

Zhang, P. and Dressler, G. R. (2013). The Groucho protein Grg4 suppresses Smad7 to activate BMP signaling. *Biochem. Biophys. Res. Commun.* 440, 454–459.

Zhang, X., Jiang, T., Ye, L., Sun, J., Wang, L., Li, J., Wu, F., Ren, S. and Gao, G. (2025). WISP3 upregulates SDCBP expression to promote the progression of non-small cell lung cancer via the TGF-β signaling pathway. *Biochem. Pharmacol.* 240, 117082.

Zondag, L. E., Rutherford, K., Gemmell, N. J. and Wilson, M. J. (2016). Uncovering the pathways underlying whole body regeneration in a chordate model, Botrylloides leachi using de novo transcriptome analysis. *BMC Genomics* 17, 114.

FIGURE LEGENDS

Figure 1. Schematic illustration of the weekly blastogenic cycle of Botryllus schlosseri. Blastogenesis occurs weekly throughout a colony's lifespan at 18 to 20 °C. Key characteristics of the illustrated colony (made up of six zooids, clustered into a single star system) are highlighted in the initial and final blastogenic stages, stage A and D, respectively. Zooids in stages A through C maintain open incurrent siphons and sustain primary buds as they undergo growth and organogenesis (not detailed). At stage D during takeover (TO) zooids close incurrent siphons and are resorbed by the primary buds. When primary buds open their siphons and begin feeding, TO concludes and the cycle begins again as primary buds assume the role of the former generation of zooids. Created in BioRender. Valdivia, C. (2026) https://BioRender.com/lfqrgvs, licensed under CC BY 4.0.

Figure 2. Changes in morphological health scores across increasing nickel concentrations over time. Mean health scores of colonies exposed to increasing concentrations of $NiCl_2$ over time (n = 30). Health score defined as the following: 0 = dead, no blood flow; 2 = very bad with heartbeat, 4 = poor with retracted ampullae, high pigmentation, and puffy tunic; 6 = fair, part poor; 8 = good with most ampullae extended, normal tunic, and normal pigmentation, 10 = great with all ampullae extended, tunic flat, clear, and normal pigmentation.

Figure 3. Photomicrographs of colonies From top to bottom, in order of pre-exposure, 24, 48, 72, and 96 hours post exposure (hpe). **(A-A””)** Control (0 mg L^{-1} nickel (II) chloride). **(B-B””)** Colony exposed to 0.1 mg L^{-1} nickel (II) chloride. **(C-C””)** Colony exposed to 100 mg L^{-1} nickel (II) chloride. Onset of ampullae retraction (red arrows) and development of hemolymph abscesses in primary buds (yellow arrows). White bars, 5 mm.

Figure 4. SOD1 activity (U mg^{-1} protein) in B. schlosseri colonies exposed to control (0), 1, or 100 mg L^{-1} nominal nickel (II) chloride for 24 or 96 hours post exposure (hpe). Points represent individual biological replicates colored by blastogenic stages. Boxplots display the median and interquartile range with whiskers extending to 1.5x the interquartile range. Mean SOD1 activity per treatment is indicated by blue diamonds. Two-way ANOVA detected a significant effect of nickel concentration on SOD1 activity ($p < 0.05$), but no effect of exposure duration or interaction ($p > 0.05$). Tukey-Kramer adjusted pairwise comparisons averaged across exposure duration were not significant ($p > 0.05$). Fisher's LSD comparisons indicated significantly elevated SOD1 enzymatic activity in colonies exposed to 1 mg L^{-1} relative to both colonies in the 0 mg L^{-1} ($p = 0.03$) and 100 mg L^{-1} ($p = 0.02$) nominal $NiCl_2$ treatments, irrespective of time post exposure. Sample size per group is indicated on the plot.

Figure 5. Clustering and heatmap of RNAseq data. Black gene symbols indicate annotation with *B. schlosseri* transcriptome. Red gene symbols indicate supplemental annotation using a non-restricted UniProt database.

Figure 6. Functional distribution of annotated differentially expressed genes (DEGs). Spider plot illustrating the number of annotated DEGs following nickel exposure assigned to major functional categories. Of the 54 total DEGs identified, 37 were successfully annotated and are represented here. Categories include extracellular matrix (ECM), vascular function, redox metabolism, innate immune response, gene regulation, cell signaling and differentiation, and cell adhesion. Values indicate the number of DEGs associated with each functional category; genes with multiple functional annotations were assigned to their most relevant primary category.

Figure 1:

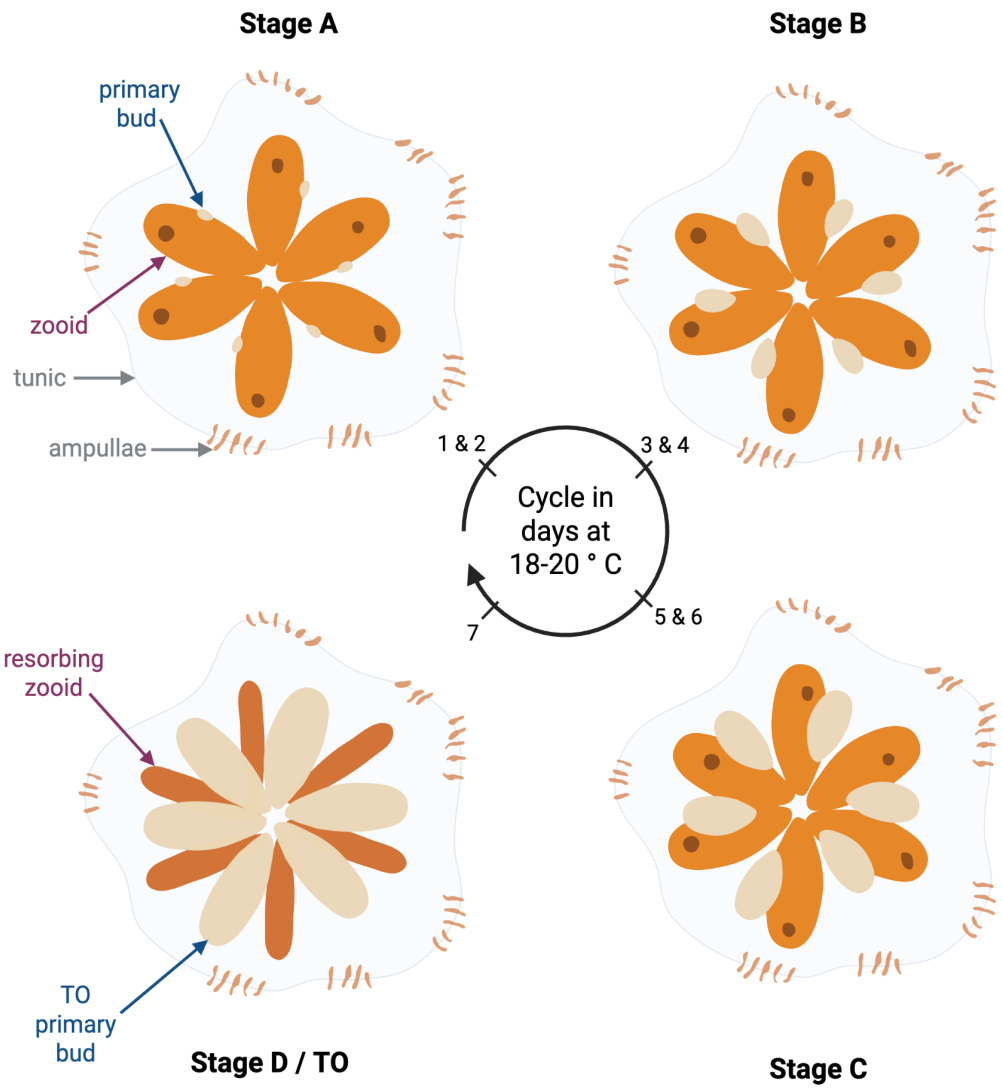
Stage A
primary bud
zooid
tunic
ampullae
Stage B
1 & 2
3 & 4
Cycle in days at 18-20 ° C
7
5 & 6
resorbing zooid
TO primary bud
Stage D / TO
Stage C

Figure 2:

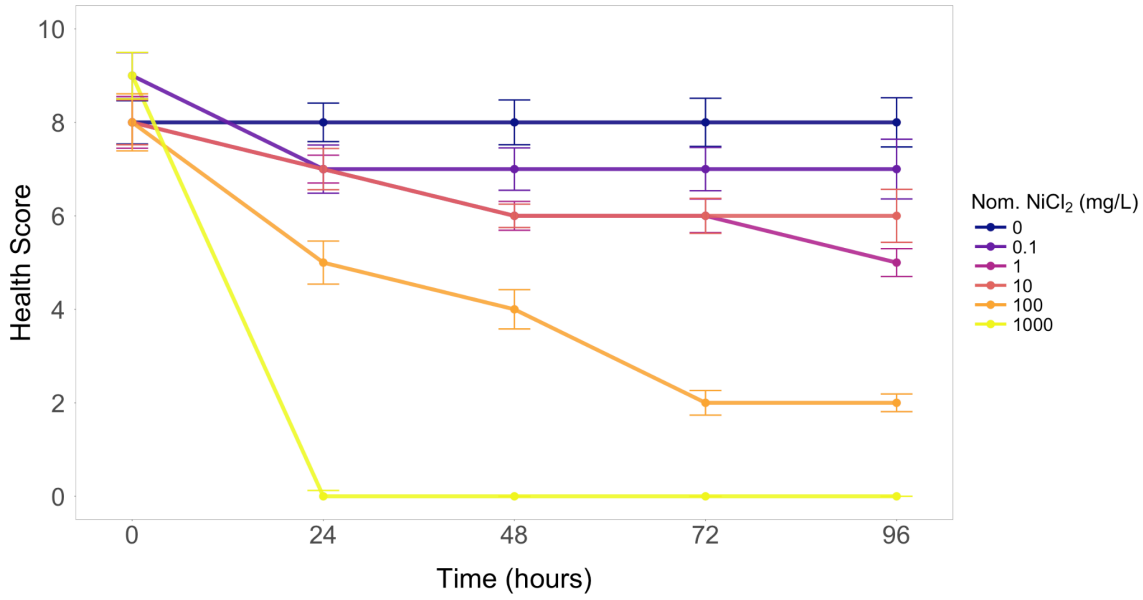
Health Score
10
8
6
4
2
0
0
24
48
72
96
Time (hours)
Nom. NiCl2 (mg/L)
0
0.1
1
10
100
1000

Figure 3:

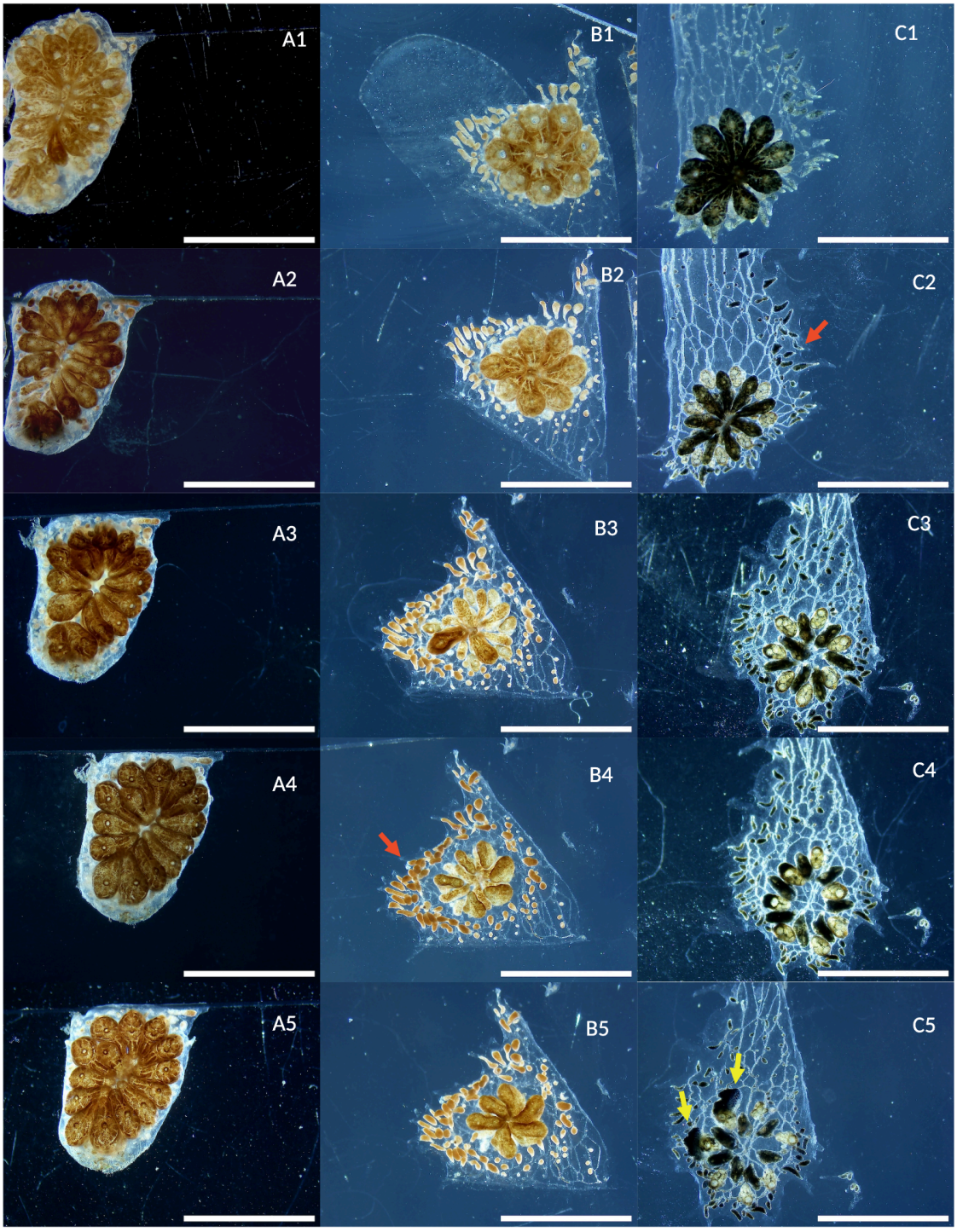

Figure 4:

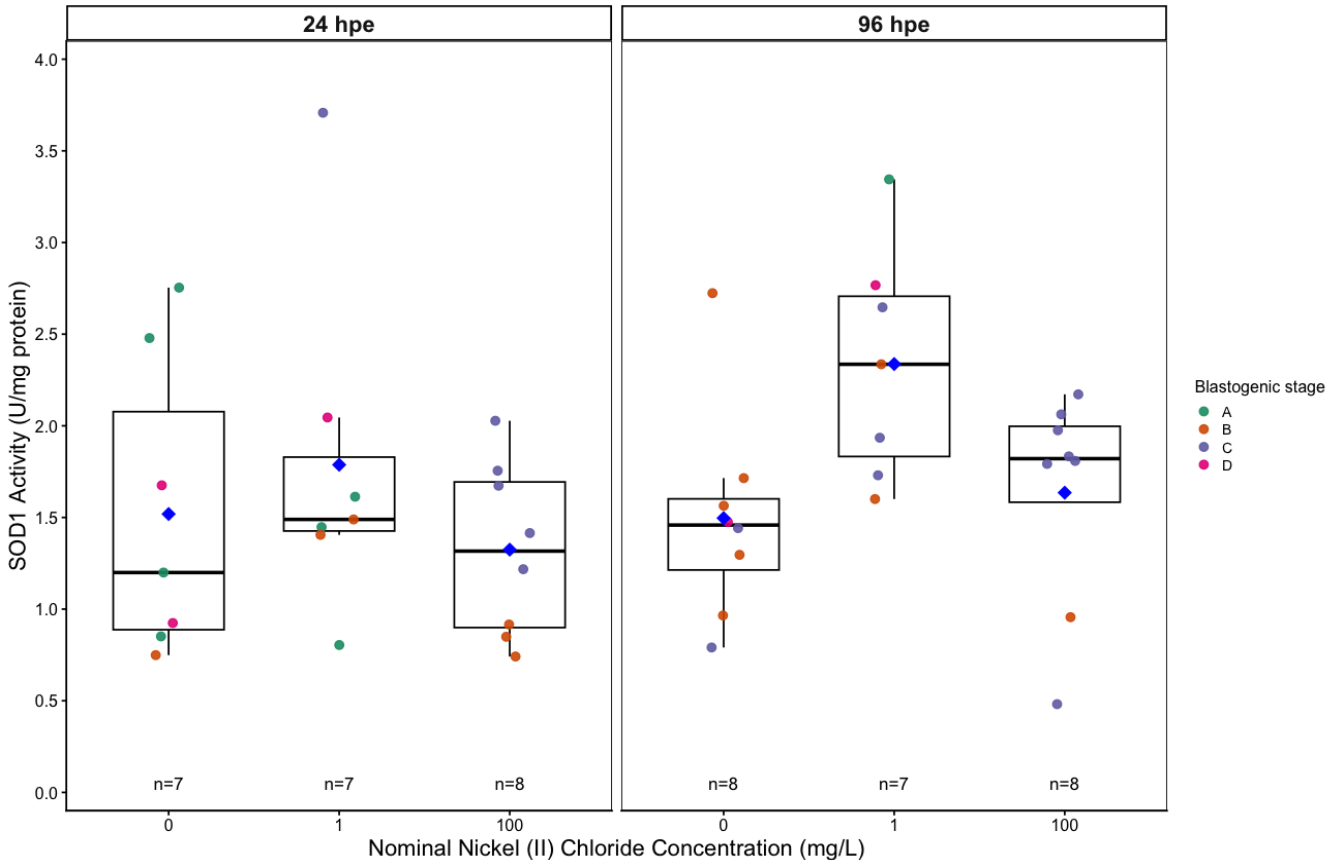
24 hpe
96 hpe
SOD1 Activity (U/mg protein)
4.0
3.5
3.0
2.5
2.0
1.5
1.0
0.5
0.0
n=7
n=7
n=8
n=8
n=7
n=8
0
1
100
0
1
100
Nominal Nickel (II) Chloride Concentration (mg/L)
Blastogenic stage
A
B
C
D

Figure 5:

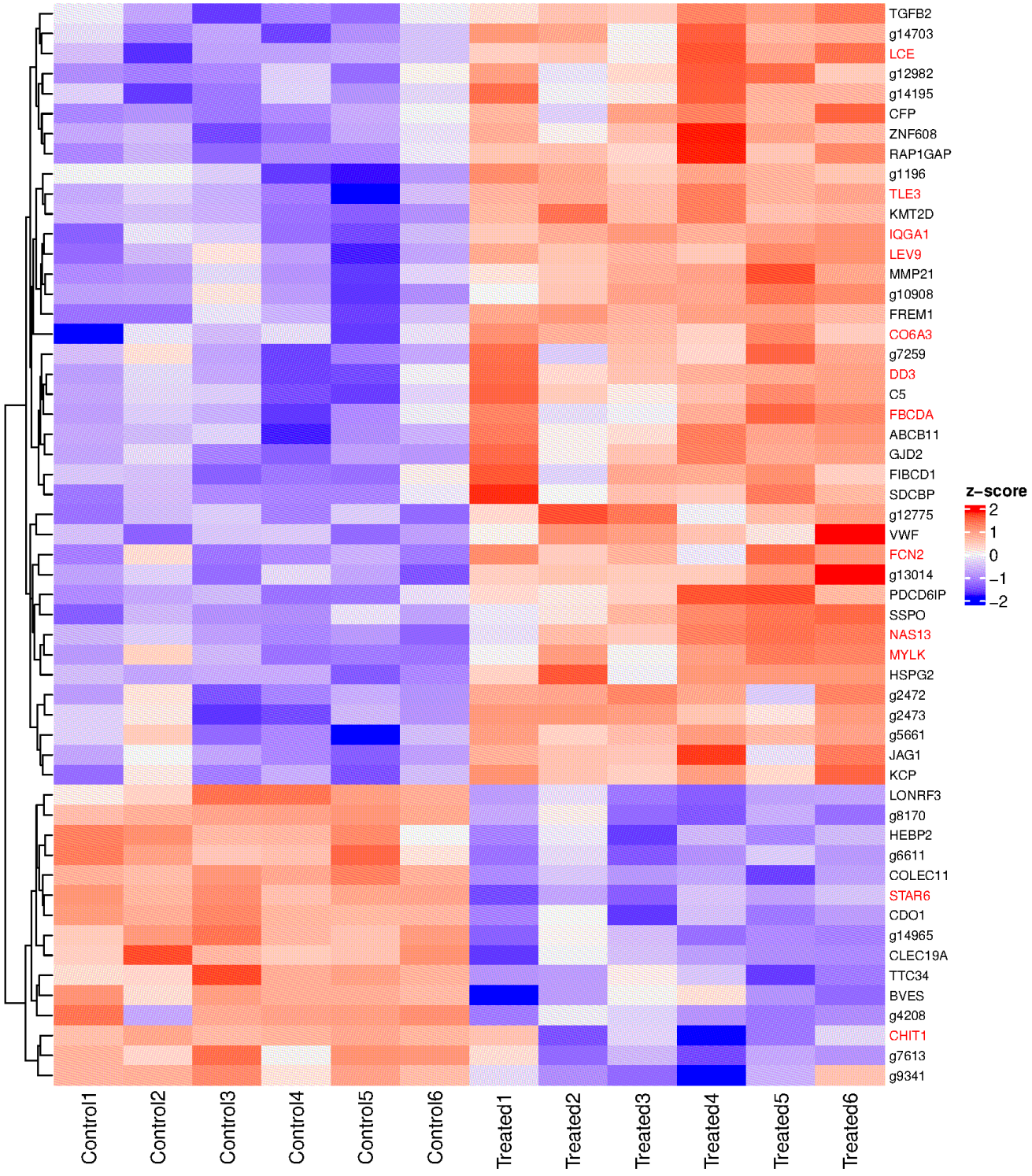
TGFB2
g14703
LCE
g12982
g14195
CFP
ZNF608
RAP1GAP
g1196
TLE3
KMT2D
IQGA1
LEV9
MMP21
g10908
FREM1
CO6A3
g7259
DD3
C5
FBCDA
ABCB11
GJD2
FIBCD1
SDCBP
g12775
VWF
FCN2
g13014
PDCD6IP
SSPO
NAS13
MYLK
HSPG2
g2472
g2473
g5661
JAG1
KCP
LONRF3
g8170
HEBP2
g6611
COLEC11
STAR6
CDO1
g14965
CLEC19A
TTC34
BVES
g4208
CHIT1
g7613
g9341
Control1
Control2
Control3
Control4
Control5
Control6
Treated1
Treated2
Treated3
Treated4
Treated5
Treated6
z−score
2
1
0
−1
−2

***Figure 6*:**

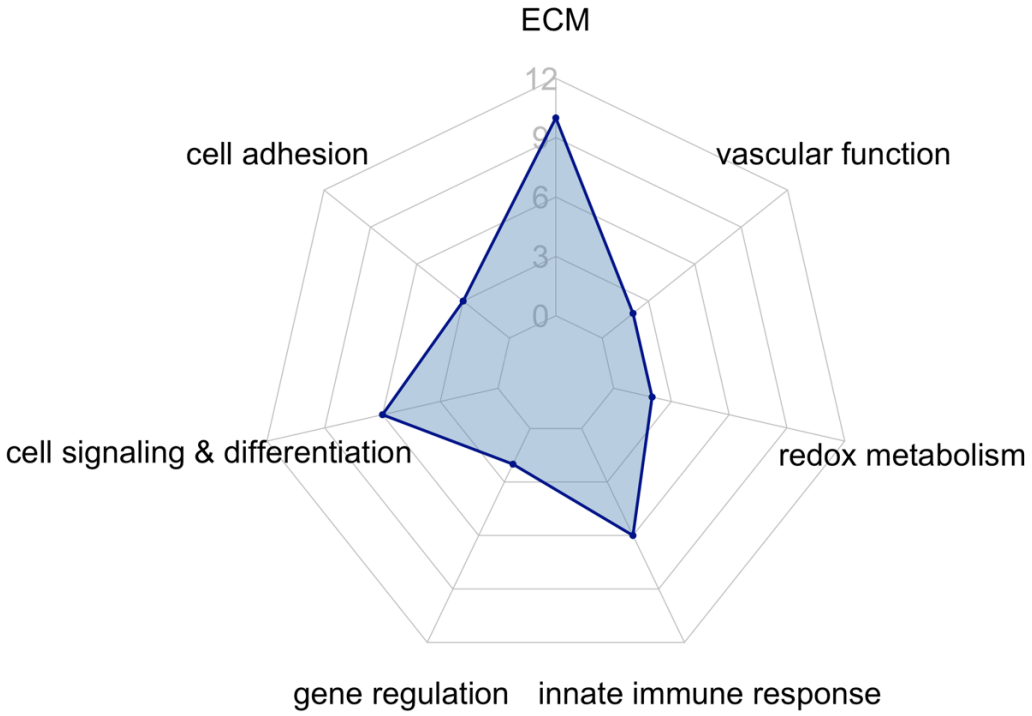
ECM
12
9
6
3
0
vascular function
redox metabolism
innate immune response
gene regulation
cell signaling & differentiation
cell adhesion

SUPPLEMENTAL FIGURE LEGENDS

Supplemental Figure 1. Schematic representation of bioinformatics workflow for DEG analysis.

Supplemental Figure 2. Best fit survivorship curve for *Botryllus schlosseri* at 24- and 96-hours post-exposure (hpe). 100% mortality observed only at the highest nickel dose. Mortality classified by cessation of blood flow throughout the colony. Red dashed intersecting lines mark crude 50% survival dose (crude-LC_{50}). Crude-LC_{50} Ni-60 values for 24-hpe and 96-hpe are calculated to be 177 and 159 mg L^{-1}, respectively.

Supplemental Figure 3. Visualization of similarity of gene expression profiles across control and nickel treated samples. Scale indicates relative weight of each sample to reflect within-group similarity.

Supplemental Figure 1:

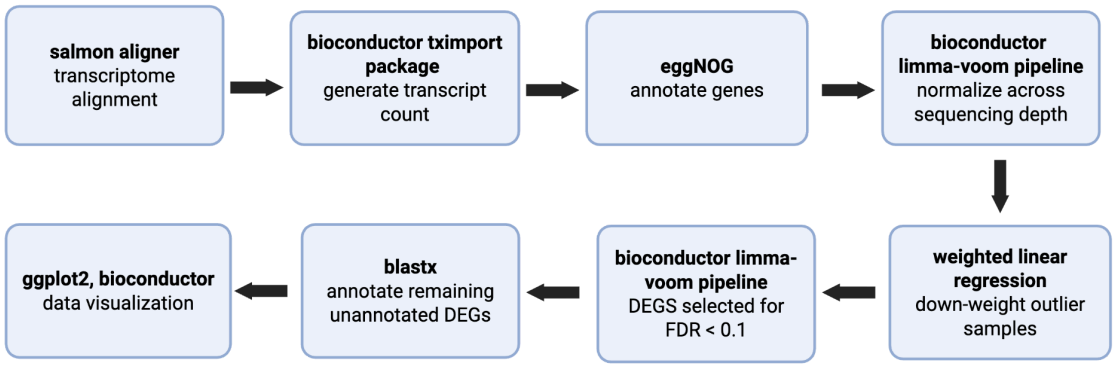

Supplemental Figure 2:

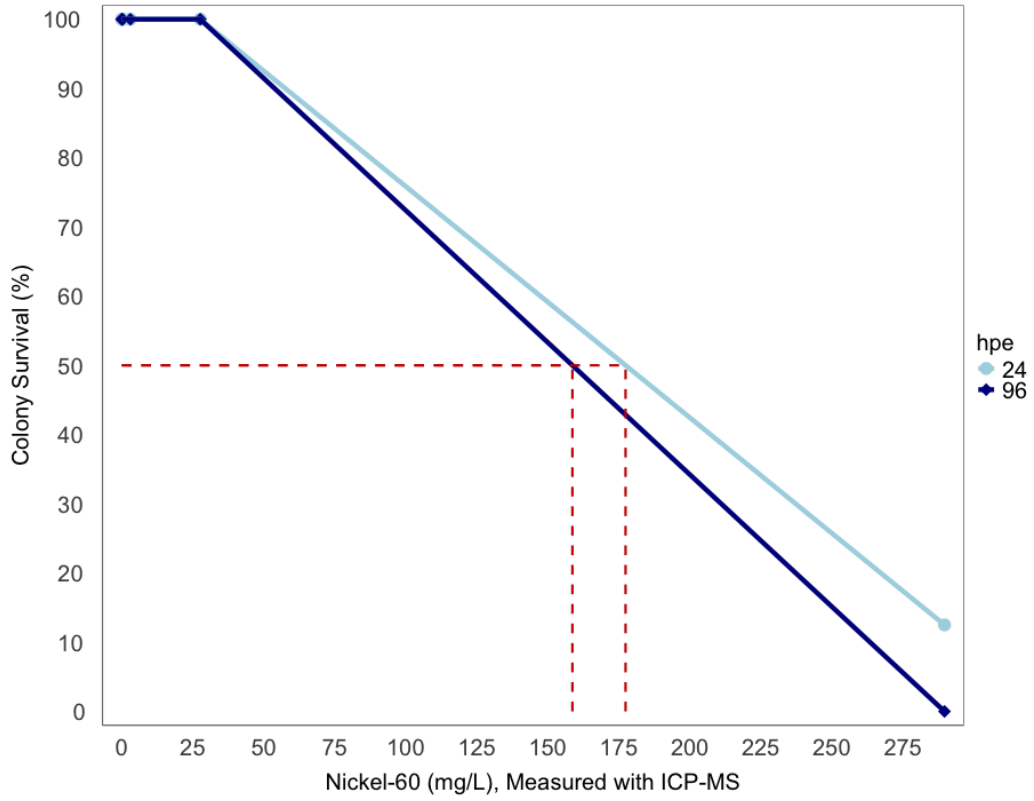

Supplemental Figure 3:

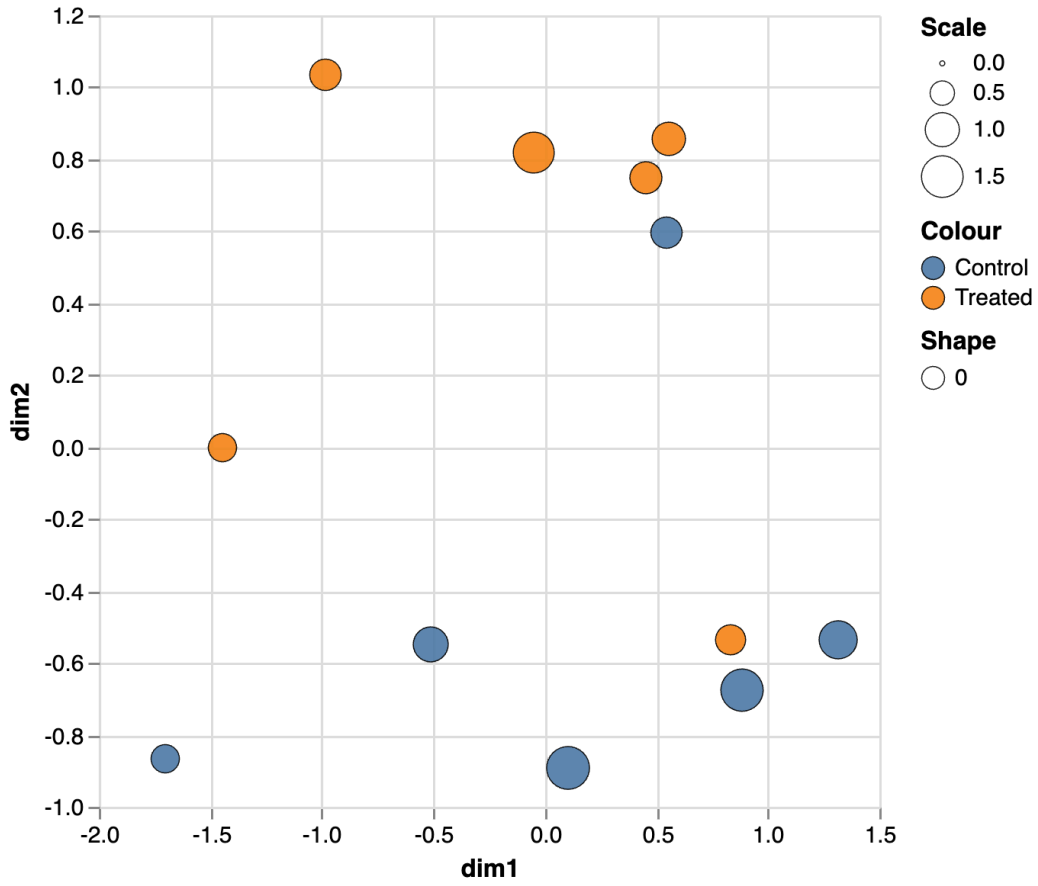

SUPPLEMENTAL TABLE LEGENDS

***Supplemental Table 1*. ICP-MS quality assurance results of measured nickel-60 (Ni-60) concentration for range-finding study exposure water samples.** Stock solutions were prepared for each of the four iterations of range-finding study and spiked water distributed for each technical replicate. Ni concentrations were below the expected nominal Ni concentrations but fell within a proportionally increasing pattern with increasing target nominal $NiCl_2$ concentrations.

***Supplemental Table 2*. ICP-MS quality assurance results of measured nickel-60 (Ni-60) concentration for RNA-seq study exposure water samples.** For each exposure vessel, exposure water was freshly prepared based on target nominal $NiCl_2$ concentrations. Measured Ni-60 concentrations were below expected nominal Ni concentrations, but consistent with measured Ni-60 concentrations of range-finding exposure water samples of the same target concentrations.

***Supplemental Table 3*. Nickel LC_{50} values reported for select marine invertebrates under seawater exposure conditions.** Reported toxicity thresholds vary widely depending on species, life stage, exposure duration, and water chemistry parameters. Relevant water chemistry parameters include temperature, salinity, pH, and seawater composition (natural seawater [NSW] versus artificial seawater [ASW]). Values contextualize the nickel tolerance observed in *B. schlosseri* in the present study.

Supplemental Table 1.

Analytical Chemistry ICP-MS Results for Range-finding Study						
Nominal NiCl2 mg/L	**Nominal Ni mg/L**	**Mean Ni-60 mg/L**	**SD Ni-60 mg/L**	**Min. Ni-60 mg/L**	**Max Ni-60 mg/L**	**Sample Size**
0	0	0.01	0.01	0	0.01	4
0.1	0.05	0.04	0.01	0.03	0.04	4
1	0.45	0.29	0.01	0.28	0.3	4
10	4.53	3.03	0.49	2.5	3.58	4
100	45.29	27.64	10.14	16.7	38.69	4
1000	452.88	289.66	30.11	261.16	319.56	4

Supplemental Table 2.

Analytical Chemistry ICP-MS Results for RNA-seq Study						
Nominal NiCl2 mg/L	**Nominal Ni mg/L**	**Mean Ni-60 mg/L**	**SD Ni-60 mg/L**	**Min. Ni-60 mg/L**	**Max Ni-60 mg/L**	**Sample Size**
0	0	0	0	0	0.01	10
100	45.29	38.07	9.13	29.06	54.44	9

Supplemental Table 3.

Species and Life Stage			**Water Chemistry Parameters**				**Assay Parameters and Results**			**Source**
Species	**Taxonomic group**	**Life stage**	**Temperature (°C)**	**Salinity (ppt)**	**Seawater Type**	**pH**	**Exposure (h)**	**Exposure Regime**	**LC50 (mg/L Ni)**	**DOI**
Botryllus schlosseri	**Tunicate (ascidian)**	**Adult**	**18**	**33**	**ASW**	**8.2**	**24**	**static**	**177**	**present study**
Botryllus schlosseri	**Tunicate (ascidian)**	**Adult**	**18**	**33**	**ASW**	**8.2**	**96**	**static**	**159**	**present study**
Allorchestes compressa	Crustacean (amphipod)	Juvenile	20	32	ASW	N/A	96	static	34	10.1016/0048-9697(94)90391-3
Babylonia areolata	Mollusk (gastropod)	Adult	24	37	ASW	7.8 to 8.2	96	static	34	10.1080/02772248.2013.864450
Crassostrea virginica	Mollusk (oyster)	Embryo	26	25	ASW	7.0 to 8.5	48	static	1	10.1007/BF00367984
Mya arenaria	Mollusk (clam)	Adult	20	20	NSW	7.8	96	static	320	10.1007/BF02097772
Asterias forbesi	Echinoderm (starfish)	Adult	20	20	NSW	7.8	96	static	150	10.1007/BF02097772
Macoma balthica	Mollusk (clam)	Adult	15	35	NSW	N/A	96	static	540	10.3354/MEPS024139

Tab 2

Potential Journal List
Journal, Impact Factor

- ➔ The science of the total environment, 8-10
  - ◆ RULES
    - *It is essential that the authors focus on only those references that are truly relevant to the work being presented.* ***STOTEN now limits the total number of references in a research paper to a total of 50*** *and in a review paper, the limit is 100.*
    - ***300 word max abstract***
    - ***You are required to provide 1 to 7 keywords*** *for indexing purposes. Keywords should be written in English. Please try to avoid keywords consisting of multiple words*